How to cite: *Angew. Chem. Int. Ed.* **2023**, *62*, e202307343
doi.org/10.1002/anie.202307343

Covalent Organic Frameworks | Hot Paper

Site-Selective Synthesis and Concurrent Immobilization of Imine-Based Covalent Organic Frameworks on Electrodes Using an Electrogenerated Acid

*Tomoki Shirokura, Tomoki Hirohata, Kosuke Sato, Elena Villani, Kazuyasu Sekiya, Yu-An Chien, Tomoyuki Kurioka, Ryoyu Hifumi, Yoshiyuki Hattori, Masato Sone, Ikuyoshi Tomita, and Shinsuke Inagi**

Abstract: Imine-based covalent organic frameworks (COFs) are crystalline porous materials with prospective uses in various devices. However, general bulk synthetic methods usually produce COFs as powders that are insoluble in most of the common organic solvents, arising challenges for the subsequent molding and fixing of these materials on substrates. Here, we report a novel synthetic methodology that utilizes an electrogenerated acid (EGA), which is produced at an electrode surface by electrochemical oxidation of a suitable precursor, acting as an effective Brønsted acid catalyst for imine bond formation from the corresponding amine and aldehyde monomers. Simultaneously, it provides the corresponding COF film deposited on the electrode surface. The COF structures obtained with this method exhibited high crystallinities and porosities, and the film thickness could be controlled. Furthermore, such process was applied for the synthesis of various imine-based COFs, including a three-dimensional (3D) COF structure.

[*] T. Shirokura, Dr. T. Hirohata, Dr. K. Sato, Dr. E. Villani, Dr. R. Hifumi, Prof. Dr. I. Tomita, Prof. Dr. S. Inagi
Department of Chemical Science and Engineering,
Tokyo Institute of Technology
4259 Nagatsuta-cho, Midori-ku,
Yokohama, Kanagawa 226-8502 (Japan)
E-mail: inagi@cap.mac.titech.ac.jp

K. Sekiya, Prof. Dr. Y. Hattori
Faculty of Textile Science and Technology, Shinshu University
Ueda, Nagano 386-8567 (Japan)

Y.-A. Chien, Dr. T. Kurioka, Prof. Dr. M. Sone
Institute of Innovative Research, Tokyo Institute of Technology
4259 Nagatsuta-cho, Midori-ku,
Yokohama, Kanagawa 226-8503 (Japan)

Introduction

Covalent organic frameworks (COFs) are two-dimensional (2D) or three-dimensional (3D) crystalline porous materials constructed by connecting organic molecules with covalent bonds.[1–3] Because they are composed of light elements and porous structures with regularly ordered molecules, they have a low density and a high surface area. Furthermore, their pore size, shape and electronic state can be easily controlled by designing the monomer molecules necessary to build the frameworks. In particular, imine-linked COFs have attracted extensive attention because of their excellent thermal and chemical stability, together with the broad monomer scope.[4] Thanks to these characteristics, imine-based COFs have been examined as materials for various applications such as gas storage and separation materials,[5–8] catalysts,[9,10] and electrode materials.[11–13]

Currently, most of these imine-based COFs are synthesized either under solvothermal conditions using water and glacial acetic acid,[14–16] or at room temperature using Lewis acid catalysts.[17] However, these methods usually produce COFs as bulk powders that generally show poor solubility in most of the common solvents, posing many challenges for their subsequent processing and molding.[18] In this context, with the aim to effectively utilize their large surface area and expand their potential range for applications, several fabrication methods for the production of 2D imine-based COF sheets and films have been reported, including exfoliation of bulk COFs into nanosheets,[19–22] use of gas-liquid[23,24] and liquid-liquid[7,25–27] interfaces, and the employment of supports acting as templates for the preparation of freestanding films.[28] In addition, some methodologies for fixing imine-based COF films onto different substrates have been developed, including the treatment of a droplet of monomer solution placed onto the substrate under solvothermal conditions,[29,30] and the use of the substrate as a template for carrying out the polymerization process while controlling the bulk reaction.[31–33]

Several attempts to use electrochemistry for synthesizing and fixing COFs on electrodes have been reported, e.g., the fabrication of COF films by electrophoretic deposition (EPD),[34–36] the production of COF films with phenazine linkages by electrochemical radical coupling reaction,[37] and the fixation of COF films by exfoliation of bulk COFs at the

cathode followed by deposition at the anode.[38] Although all of these methods successfully allow the production of COF films onto the electrode surface, some issues remain, such as the limitations of ionic building blocks for EPD, the low crystallinity or porosity, and the need of multiple synthetic steps to chemically synthesize COFs as precursors.

Here, we focus on an electrogenerated acid (EGA) generated at the electrode surface by electrochemical oxidation and propose to use it as a Brønsted acid catalyst for the condensation reaction of amines and aldehydes to form imine bonds. In general, an EGA is generated by the oxidation of a trace amount of water in an aprotic organic electrolytic solution and acts as a strong Brønsted acid because it is not hydrated.[39] In addition, because it can be generated in the proximity of the electrode surface, localized reactions can be achieved near the electrode. Among EGAs, 1,2-diphenylhydrazine (DPH) is known to release a proton at a potential lower than that of water oxidation and to work as an acid, e.g., it has been used for the removal of the *t*-BOC protecting group at any position for peptide array synthesis[40] and for depositing organic molecular films on glassy carbon (GC) electrodes.[41,42]

In this work, we have successfully achieved the bottom-up synthesis of imine-based COF films onto the electrode surface by using an EGA as a catalyst for the condensation reaction of amine and aldehyde monomers (Figure 1). In this reaction system, DPH was chosen and employed as an EGA source thanks to low oxidation potential, since the oxidation of the EGA source must proceed preferentially compared to the oxidation of the monomers. Film-like deposits were obtained onto the electrodes immersed in an electrolyte containing the monomers and DPH by the potential-sweep method. Fourier transform infrared spectroscopy (FT-IR) and ^{13}C cross-polarization/magic angle spinning nuclear magnetic resonance spectrometry (CP-MAS ^{13}C NMR) measurements revealed that the resulting deposits were COFs composed of imine bonds. The high crystallinities and porosities of these COFs were evaluated by small-angle X-ray scattering (SAXS) and N_2 gas adsorption/desorption measurements. Furthermore, we additionally applied this methodology for the synthesis of triazine-based COFs and 3D COF structures. The use of EGA in the COFs fabrication process has been demonstrated to be not only an excellent method for fixing COFs onto the electrodes, but also an innovative synthetic approach based on sustainable electrosynthesis, thanks to features such as the low environmental impact, the short reaction time under mild conditions, and the easy purification process. Such novel synthetic method for imine-based COFs fabrication proposed in this work is expected to be a promising process technology for COF-based applications, such as functional modified electrodes and sensing devices.

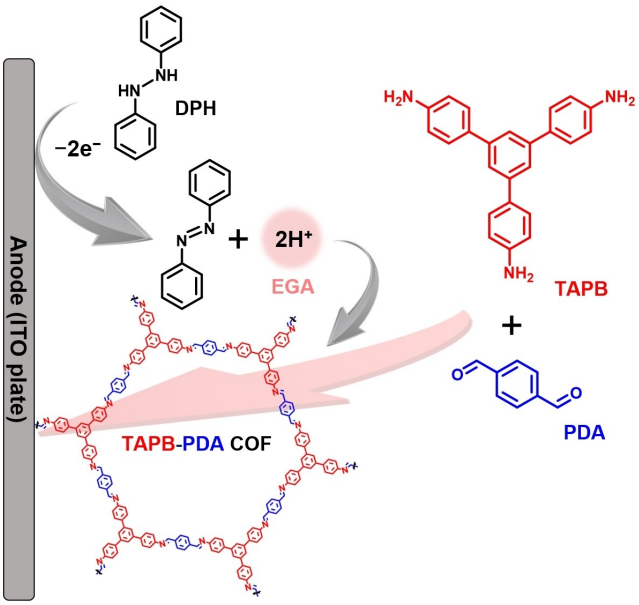

Figure 1. Concept of this study: the use of electrogenerated acid (EGA) for COFs synthesis and their immobilization onto the electrode surface.

Results and Discussion

We initially investigated the electrochemical behavior of DPH and its accompanying change in acidity near the electrode surface. Firstly, cyclic voltammetry (CV) of DPH was performed in a nitromethane ($MeNO_2$) solution containing tetrabutylammonium hexafluorophosphate (Bu_4NPF_6). An irreversible oxidation peak was observed with the onset potential located at around 0.3 V vs. Ag/Ag^+ (Figure S1), indicating that the electrochemical oxidation of DPH induced its chemical transformation to azobenzene through release of protons. The application of multiple potential sweeps in the potential range between −0.5 to 0.5 V gave rise to a gradual increase of the current (Figure 2a). To visualize such electrochemical reaction of DPH, the potential sweep was performed with the addition of methyl yellow as a pH indicator, which colors red under acidic conditions (Figure 2b). As a result, the working electrode surface turned red after one cycle, and the colored portion diffused into the solution with repetitive sweep cycles. Without DPH, such color change of the electrode surface was not observed. Furthermore, when DPH solutions were electrolyzed using the working electrode wrapped with pH test papers, only the area covering the electrode surface showed a red color corresponding to pH 2–3 (Figure 2c). The structural changes of DPH by electrochemical oxidation were subsequently analyzed by ^1H NMR. The electrolysis of DPH was performed for 1.7 F mol^{-1} either with the constant-potential method at 0.5 V vs. Ag/Ag^+ or with the constant-current method. Comparing the ^1H NMR spectra of DPH before and after electrolysis, the signals of DPH decreased while the signals of azobenzene appeared (Figure S2). In other words, DPH released protons upon electrochemical oxidation and got converted to azobenzene as expected. These results indicate that DPH is electrochemically oxidized at around 0.3 V and the consequent release of protons causes the pH near the electrode surface

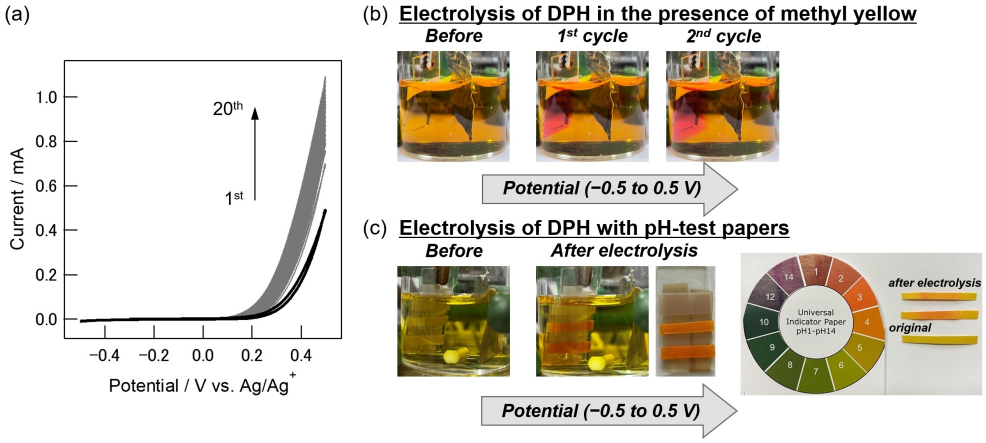

Figure 2. a) Cyclic voltammograms of DPH (20 mM) in 0.1 M $Bu_4NPF_6/MeNO_2$ using an ITO working electrode (10 mm×10 mm), a Pt counter electrode (20 mm×20 mm) and an Ag/Ag^+ reference electrode for 20 cycles at a scan rate of 20 mV s^{-1}. Photographs of b) the cell during electrolysis in the presence of methyl yellow and c) the cell during electrolysis with the ITO working electrode wrapped with pH test papers.

to decrease, suggesting that DPH can work as a good EGA source.

For the synthesis of imine-based COFs using an EGA as an acid catalyst, it is necessary to consider the oxidation potential of the monomer molecules consisting of the COFs structure. Linear sweep voltammetry (LSV) of 1,3,5-tris(4-aminophenyl)benzene (TAPB) as an amine monomer, terephthalaldehyde (PDA) as an aldehyde monomer and DPH as an EGA source was performed in 0.1 M $Bu_4NPF_6/MeNO_2$ (Figure 3a). These voltammograms show that PDA does not undergo any redox reactions in the potential range between −0.5 and 1.2 V vs. Ag/Ag^+. On the other hand, the oxidation of DPH and TAPB proceeds at around 0.3 V and 0.35 V, respectively. Therefore, the oxidation of DPH is most likely to occur at a lower potential to generate the acid catalysts.

Subsequently, we examined the solvent composition for the electrolysis. A mixed solution of 1,4-dioxane and mesitylene, comsmonly used in the chemical synthesis of COFs, was the first candidate, but the solution containing 0.1 M Bu_4NPF_6 was found to have very low conductivity (0.039×10^{-3} S m^{-1}) and was not suitable as an electrolyte. Therefore, we examined several organic solvents containing 0.1 M Bu_4NPF_6 for CV measurements and constant-potential electrolysis (0.2 V or 0.4 V) of TAPB, PDA, and DPH (Figure S3, Table S1). Due to the low solubility of the substrates in ethanol (EtOH), the current observed by the CV measurements was low, and no deposit was obtained on the electrode after the constant-potential electrolysis. When using tetrahydrofuran (THF), dichloromethane, or chloroform, only a trace amount of deposits was obtained on the electrode. This result may be attributed to the high solubility of the generated oligomers and COFs in these solvents. The currents observed in dichloromethane and chloroform were low, suggesting that the electrochemical oxidation of DPH did not proceed sufficiently. For dimethylformamide (DMF)

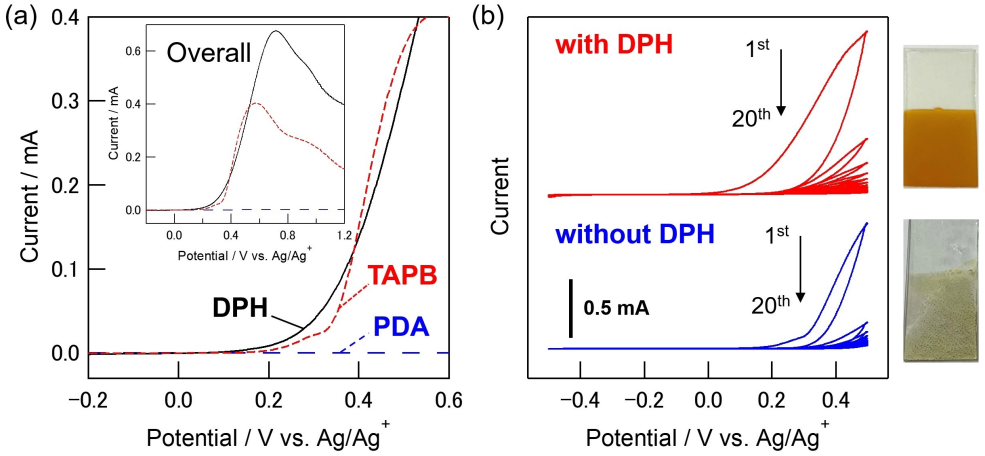

Figure 3. a) Linear sweep voltammograms of TAPB, PDA, and DPH (5 mM) in 0.1 M $Bu_4NPF_6/MeNO_2$. b) Cyclic voltammograms of TAPB and PDA with and without DPH, and photographs of the as obtained ITO electrodes. The electrolysis was performed using an ITO working electrode (10 mm×10 mm), a Pt counter electrode (20 mm×20 mm) and an Ag/Ag^+ reference electrode for 20 cycles at a scan rate of 20 mV s^{-1}.

and dimethyl sulfoxide (DMSO), the counter electrode became black immediately after starting the electrolysis, followed by the generation of black suspension in the entire solution, and no deposition was obtained on the electrode. Similarly, when acetonitrile (MeCN) or acetone was used, the entire solution was suspended during electrolysis, but only a small amount of deposit was obtained on the electrode. When $MeNO_2$ was used, a red thin film formed on the electrode from the early stages of the electrolysis, yielding an amount of deposits that could be collected with a spatula. There were no suspended solids in the electrolyte, and the deposit was obtained only on the electrode surface. Therefore, $MeNO_2$ was selected as the solvent for the electrolysis to be employed in this study.

As a next step, we investigated the applied potential and electrolyte concentrations by constant-potential electrolysis using $MeNO_2$ as a solvent. The investigations performed between 0.2 V and 0.5 V showed that a deposit was obtained on the electrode only above 0.3 V (Table S2). It was also found that the use of a low concentration of monomers (Entries 5 and 6) did not yield any deposit on the electrode, and that decreasing the DPH concentration also decreased the amount of deposit produced (Entries 7 and 8). According to these results, the optimal substrate concentrations were determined to be TAPB 10 mM, PDA 15 mM, and DPH 20 mM.

After these preliminary investigations, we also attempted to carry out the electrolysis of the substrates by the potential-sweep method. As shown in Table S3, the optimization of the electrochemical parameters was investigated by changing the potential range, the number of sweep cycles and the scan rate. In the conditions shown in Entries 1 and 2, almost no deposit was observed on the electrode when the potential was swept at values below 0.2 V. However, by increasing the potential range up to 0.3 V, some deposit was obtained on the electrode (Entry 3). When the potential was swept until 0.5 V, a thick uniform deposit covered the entire electrode surface and the obtained amount was greater than the one obtained with the constant-potential electrolysis (Entry 4). Nevertheless, it was found that the amount of deposit decreased by increasing the scan rate, as shown in Entries 5 and 6. Based on these results, we adopted the electrochemical parameters of Entry 4 as the optimal conditions for the electrolysis.

Figure 3b shows the cyclic voltammograms and photographs of the ITO electrodes after electrolysis under the optimized conditions. An oxidation current was observed in the solution containing DPH (red plot) together with the deposition of a film onto the electrode surface. Although the color of the deposit appeared reddish during the electrolysis, a uniform yellow film was obtained after rinsing with the organic solvent. The amount of deposit increased by repetitive sweep cycles even if the current decreased, presumably due to the low conductivity of the deposit formed onto the electrode. A control experiment was performed in the absence of DPH (blue plot) and no deposit was obtained although the oxidation current of TAPB was observed at slightly higher potential than that of DPH. Therefore, DPH was preferentially oxidized to generate an acid for catalyzing imine bond formation between TAPB and PDA monomers.

The deposits obtained on the electrode (Figure 3b) were examined to evaluate their physical properties and the molecular and crystalline structures. FT-IR analysis revealed the imine (C=N) stretching band at 1620 cm^{-1} (Figure 4a and S4). CP-MAS ^{13}C NMR analysis provided a signal at around 160 ppm assignable to imine bonds (Figure 4b). XPS analysis showed the generation of imine bond based on the C1s and N1s peaks (Figure S5). These results confirmed that the deposits obtained onto the electrode surface are covalent organic frameworks consisting of TAPB and PDA connected by imine bonds (TAPB-PDA COF). In addition, the stretching band observed at 1696 cm^{-1} in the IR spectrum and the signal at around 190 ppm in the CP-MAS ^{13}C NMR spectrum can be attributed to the aldehyde (CH=O) group, suggesting the presence of a small amount of unreacted aldehyde terminals.

Crystalline structure analysis was performed using small-angle X-ray scattering (SAXS) measurements (Figure 4c). The SAXS diffraction patterns of the TAPB-PDA COF showed the strongest diffraction peak at $2\theta = 2.83°$, $d = 3.13$ nm, corresponding to the (100) plane. The diffraction peaks were also observed at $2\theta = 4.91°$, 5.66°, 7.50°, 10.01° and 12.40° corresponding to (110), (200), (210), (220), and (320) planes, respectively.[17] In addition, the peak in the (001) plane at $2\theta = 25.40°$, $d = 0.35$ nm corresponded to the interlayer stacking of the 2D COF. Therefore, the TAPB-PDA COF obtained on the electrode possesses a crystalline structure.

The specific surface area of the COF was calculated by nitrogen gas (N_2) adsorption/desorption measurement. The N_2 adsorption isotherm shown in Figure 4d had the characteristic shape of porous COF materials. The Brunauer–Emmett–Teller (BET) plot was a linear plot and the experimental BET surface area was 832 $m^2 g^{-1}$. Furthermore, the pore size distribution calculated by the non-local density functional theory (NLDFT) method was found to be in the range of 20 to 40 Å, corresponding to the expected pore size (34 Å) (Figure 4e).[20]

We also attempted to synthesize COF films onto different electrode materials with the optimized set of conditions determined in Figure 3b. On platinum (Pt), gold (Au), and GC electrodes, crystalline COF films were obtained similarly to that obtained on the ITO electrode (Figure S6). This result indicates that imine-based COFs can be synthesized and be immobilized onto the electrode surface with the EGA-catalyzed method irrespective of the electrode material.

The morphology of the COF material was analyzed by scanning electron microscopy (SEM) (Figure 5a). The TAPB-PDA COF film obtained with the potential-sweep method (20 cycles) onto the ITO electrode was found to be an aggregation of submicrometer-sized particles having a thickness of ca. 100 μm. In addition, the relationship between the number of cycles and COF film thickness was also investigated (Figure 5b). The film thickness increased linearly with the number of cycles until 20 cycles, indicating that it is possible to control the thickness of the COF films

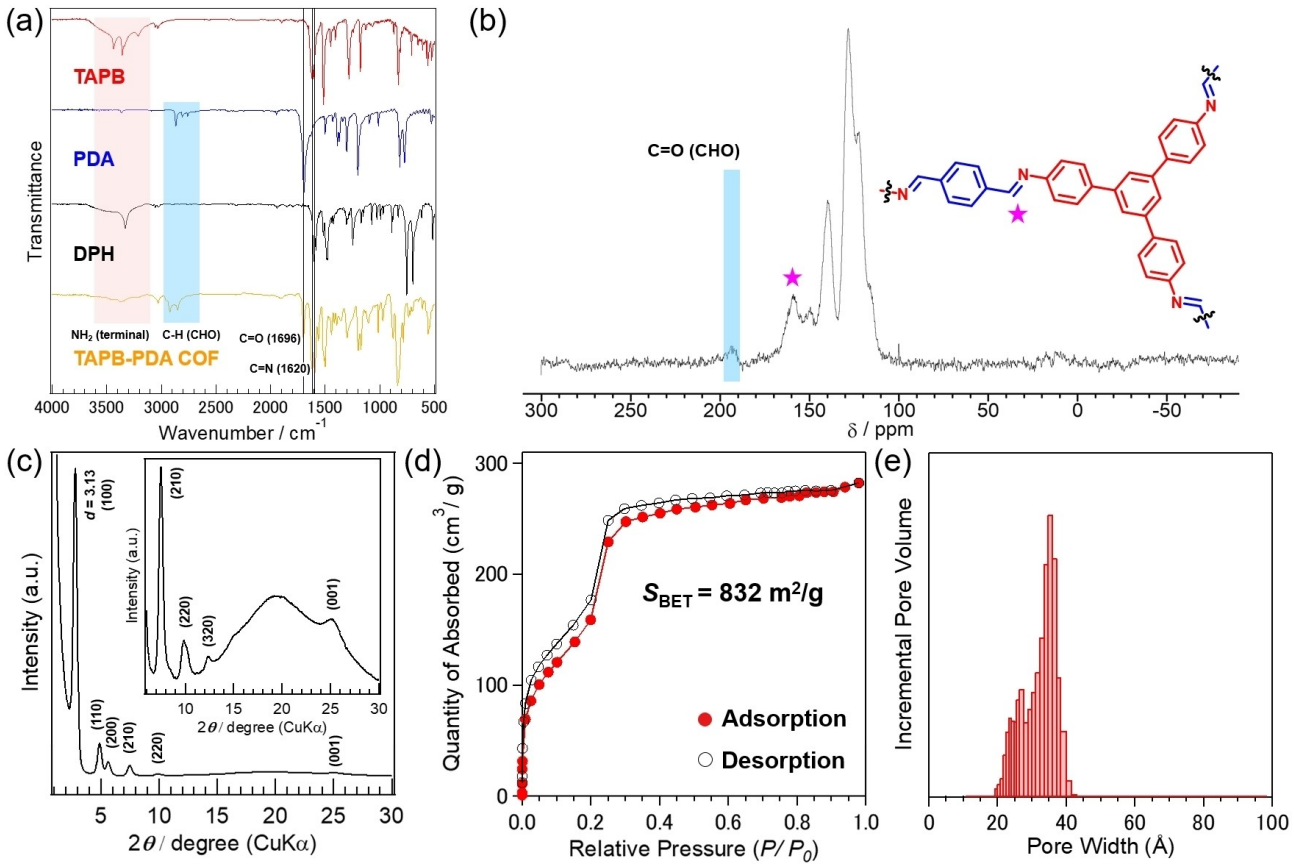

Figure 4. Structural characteristics and properties of the TAPB-PDA COF. a) FT-IR spectra of TAPB, PDA, DPH and the TAPB-PDA COF. b) CP-MAS ^{13}C NMR spectrum of the TAPB-PDA COF. c) SAXS diffraction patterns, d) N_2 adsorption (filled circles) and desorption (empty circles) isotherms (77 K) and e) NLDFT-calculated pore size distribution of TAPB-PDA COF. The pore size and their distributions were determined using DFT models of cylinder carbon. The sample was rinsed with MeCN, MeOH and hexane, and activated by supercritical CO_2 drying.

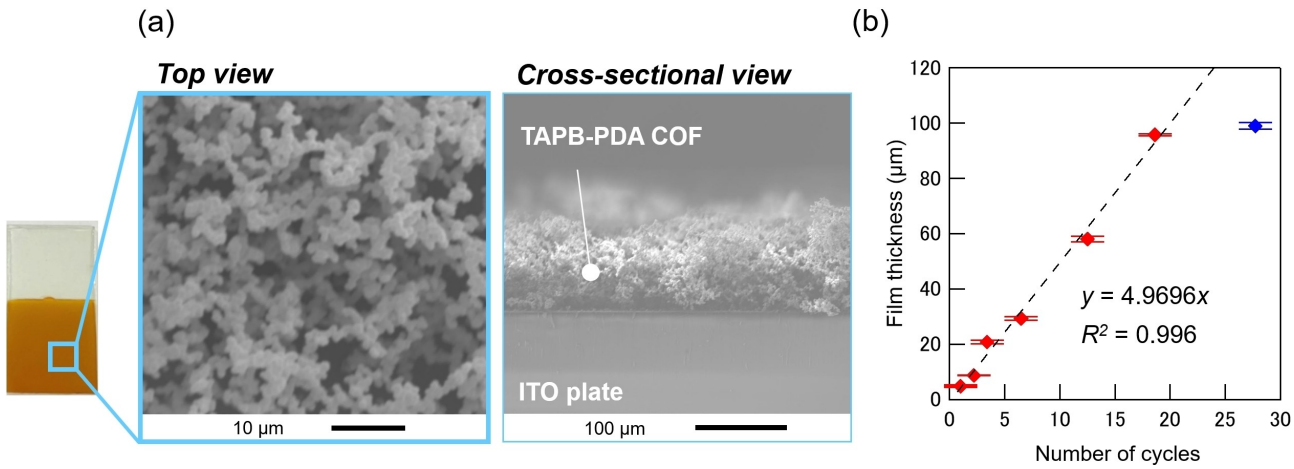

Figure 5. Morphological characteristics of the TAPB-PDA COF film. a) SEM images and b) dependency of the thickness vs the number of cycles in the potential sweep method. The film thickness was calculated from the cross-sectional SEM images.

formed onto the electrode by the EGA method up to ca. 100 μm. This relationship is believed to be established by the interplay of the EGA and the coverage of the electrode surface with a COF film with low conductivity. However, for thickness greater than 100 μm or for larger numbers of cycles, the film growth was suppressed (see the blue diamond in Figure 5b) probably due to the decrease in proton generation at such a late stage (Figure 3a with DPH) and the diffusion of Brønsted acid catalysts into the bulk electrolyte.

Thermogravimetric analysis (TGA) revealed the high thermal stability of TAPB-PDA COF (Figure S7). Contact angle measurements of a water droplet on the COF film showed a contact angle value of 135° (Figure S8), suggesting that this high hydrophobicity can be related to the agglomerated structure of the COF film.

To establish the generality of the synthetic protocol for imine-based COFs electrosynthesis using the EGA method, we also attempted to synthesize COFs with imine bonds consisting of different monomer combinations. Specifically, TAPB, 4,4′,4″-(1,3,5-triazine-2,4,6-triyl)trianiline (TAPT) and tetrakis(4-aminophenyl)methane (TAPM) were used as amine monomers, while DPA and 2,5-dimethoxybenzene-1,4-dicarboxaldehyde (OMePDA) were examined as aldehyde monomers (Figure 6).

Exploiting the optimal conditions for TAPB-PDA COF synthesis, we tried to synthesize TAPB-OMePDA COF consisting of the methoxy-introduced OMePDA monomer. The CV measurements clarified that OMePDA was redox inactive in the potential range between −0.5 to 1.2 V vs. Ag/Ag^+, like PDA (Figure 7a). Therefore, the potential-sweep electrolysis of TAPB and OMePDA with DPH in 0.1 M $Bu_4NPF_6/MeNO_2$ was performed to afford a yellow deposit on the electrode (Figure 7e).

Regarding the synthesis of triazine-based COFs and 3D COFs, it was necessary to survey the suitable solvent again because the amine monomers, TAPT and TAPM, were insoluble in $MeNO_2$, which was used for TAPB-PDA COF synthesis. Upon solvent screening, both TAPT and TAPM were found to be soluble in DMF and THF. When THF was used, the bottom of the solution changed to red during the electrolysis, but no deposit formed on the electrode or in the solution. On the other hand, DMF was found to be a suitable solvent for COF synthesis using these monomers, as evidenced by the successful formation of the COF films using the potential-sweep method (Figures 7f–h). LSV analysis suggested that DPH is preferentially oxidized in the presence of amine and aldehyde monomers (Figures 7b–d). Interestingly, in these three cases, the current in the voltammograms hardly decreased, even though the electrodes were covered with deposits by repeated sweep cycles. This result is expected to be due to less high resistance of

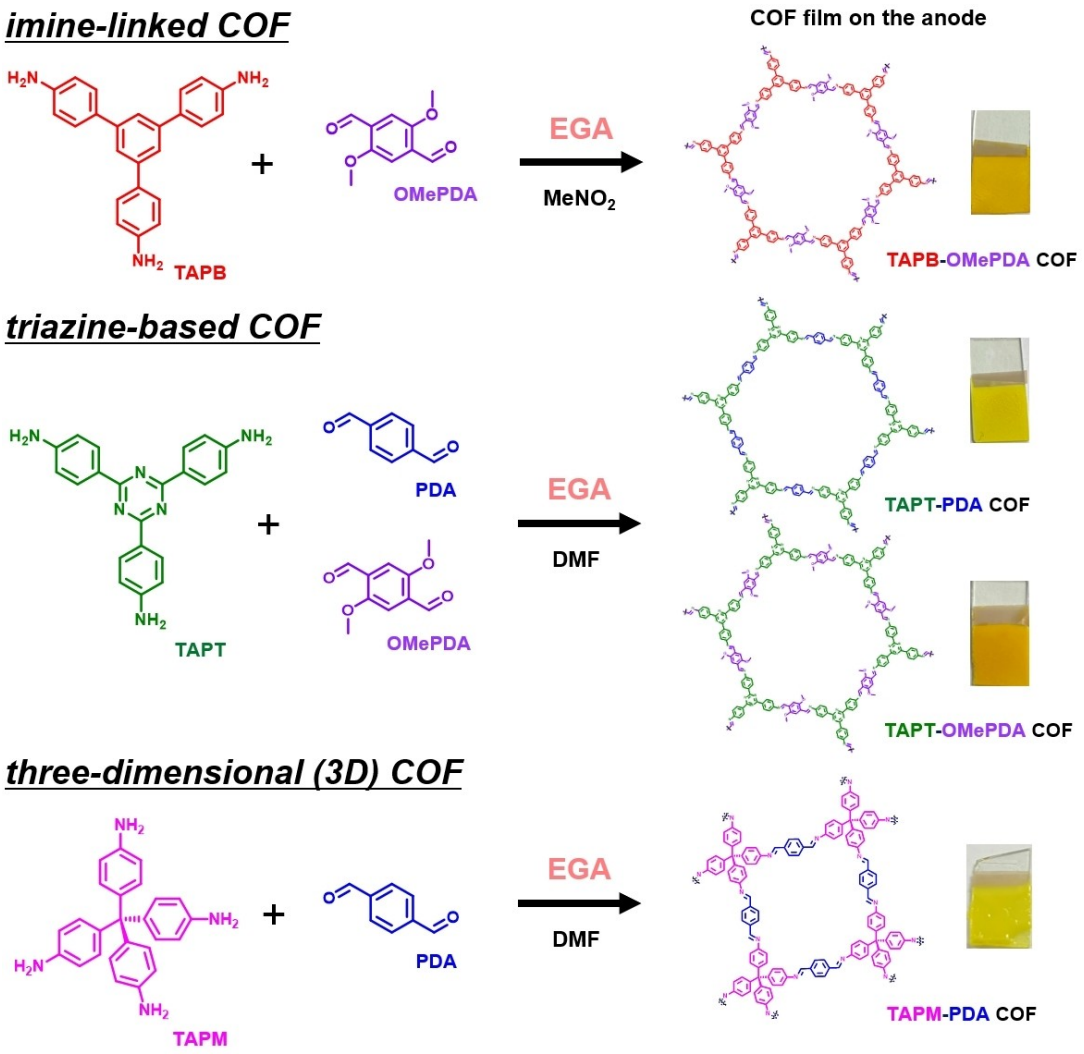

Figure 6. Overview of the synthetic pathways for TAPB-OMePDA COF, triazine-based COFs and three-dimensional (3D) COF.

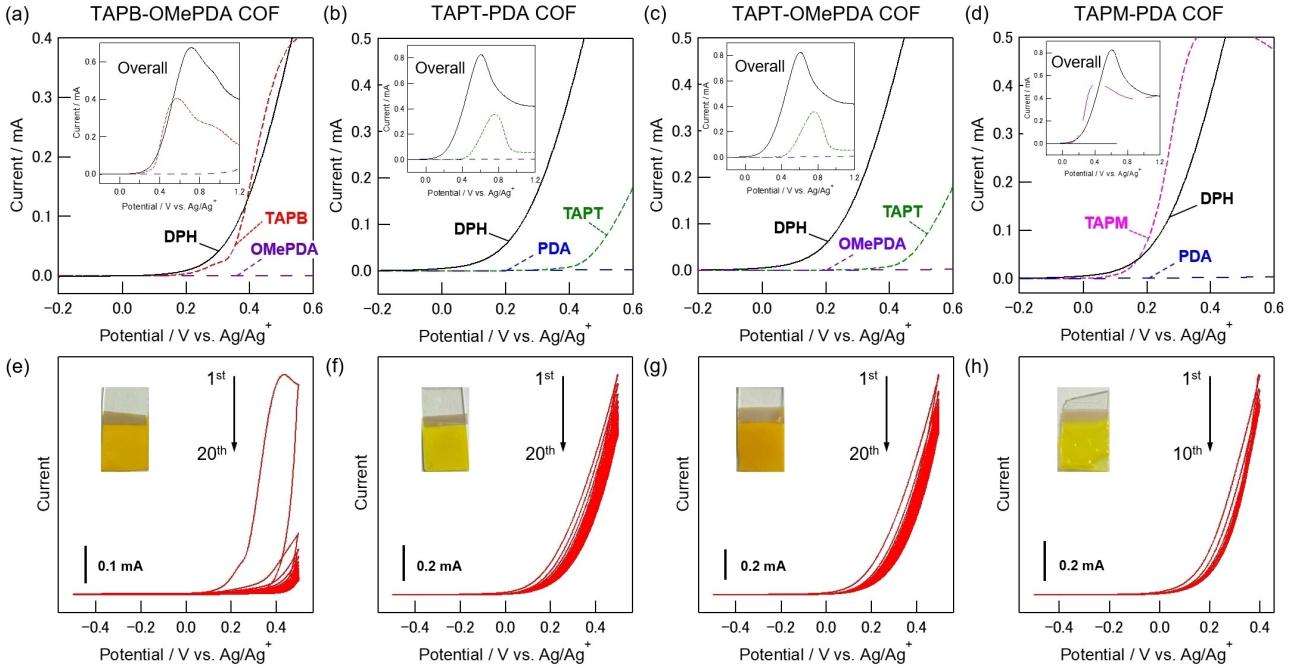

Figure 7. Linear sweep voltammograms of a) TAPB, OMePDA and DPH in 0.1 M $Bu_4NPF_6/MeNO_2$, b) TAPT, PDA and DPH, c) TAPT, OMePDA and DPH, d) TAPM, PDA and DPH in 0.1 M Bu_4NPF_6/DMF. Cyclic voltammograms during the synthesis of e) TAPB-OMePDA COF in 0.1 M $Bu_4NPF_6/MeNO_2$, f) TAPT-PDA COF, g) TAPT-OMePDA COF, h) TAPM-PDA COF in 0.1 M Bu_4NPF_6/DMF, including photographs of the corresponding COFs films onto the ITO electrodes. The electrolysis was performed by the potential-sweep method at a scan rate of 20 mV s^{-1} using an ITO working electrode (10 mm×10 mm), a Pt counter electrode (20 mm×20 mm) and an Ag/Ag^+ reference electrode for 20 cycles (e, f, g) and 10 cycles (h).

the deposits on the electrodes. For the TAPM-PDA COF synthesis, the number of potential-sweep cycles was optimized to be 10 because the COF film became too thick with 20 cycles and peeled off from the electrode when it was removed from the electrolyte.

Structural characterization, crystal structure analysis, and physical properties of the deposits obtained on the electrode by the potential-sweep method using DPH were evaluated (Figures 7e–h). The FT-IR spectra of TAPB-OMePDA COF, TAPT-PDA COF, TAPT-OMePDA COF, and TAPM-PDA COF show the C=N stretching band at 1617 cm^{-1}, 1624 cm^{-1}, 1615 cm^{-1}, and 1623 cm^{-1}, respectively (Figures 8a and S9), while the characteristic signal at around 150–160 ppm was observed in the CP-MAS ^{13}C NMR

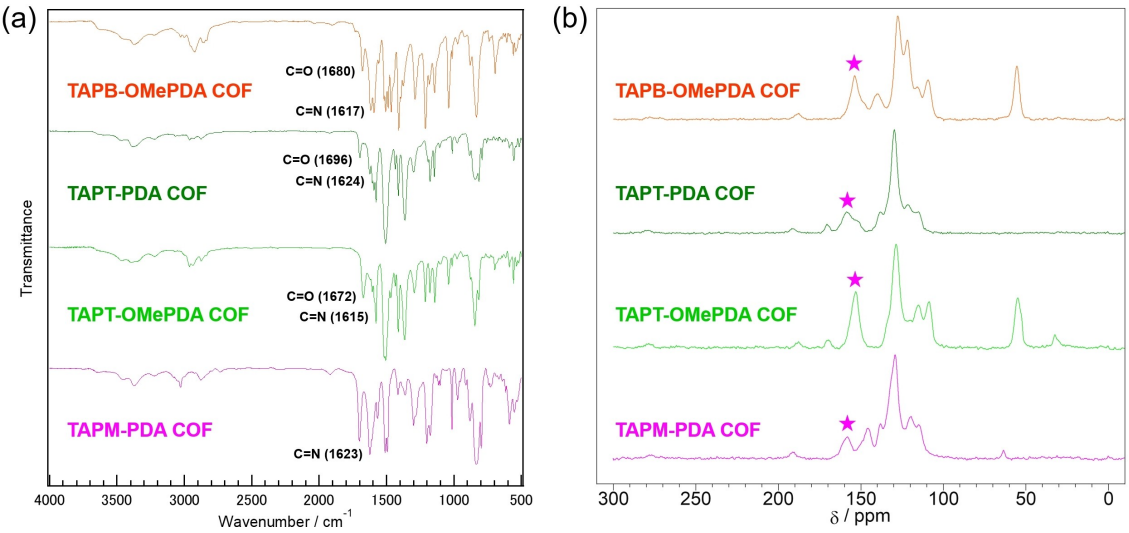

Figure 8. a) FT-IR spectra and b) CP-MAS ^{13}C NMR spectra of TAPB-OMePDA COF, TAPT-PDA COF, TAPT-OMePDA COF and TAPM-PDA COF. The star symbol indicates the peak assigned to the C=N carbon.

spectra, which is attributed to the C=N carbon (Figure 8b). In addition, characteristic signals ascribable to the carbons of each monomer component observed in the NMR spectra support the expected compositions of the COFs (Figure S10). XPS analysis also implied the generation of imine bond (Figure S11).These results suggest that the deposits obtained onto the electrodes are imine-based COFs consisting of the various combination of amine and aldehyde monomers.

To ensure the clarity regarding the competitive oxidation of DPH and the amine monomers, the TAPT-OMePDA film was prepared under a milder condition where the potential sweep range was between −0.5 and 0.3 V vs. Ag/Ag^+ (Figure S12). Since TAPT was not oxidized in this potential range, only DPH was involved in the oxidation. The yellow film was successfully obtained and identified as TAPT-OMePDA. This result strongly supports the proposed EGA-initiated polymerization mechanism.

The 2D COFs were found to have crystallinities by SAXS analysis (Figure S13) and porosities by N_2 adsorption isotherm measurements (Figure S14). On the other hand, for the TAPM-PDA COF with 3D structure, the characteristic peaks were observed at $2\theta = 8.49°$, 11.23°, 18.20°, and 21.31° in the SAXS pattern. This is consistent with the patterns obtained by chemical synthesis of the TAPB-PDA COF with heating reported in two previous reports, which does not have a porous structure.[43,44] In these reports, it was clarified that this effect was due to the distortion of the porous structure induced by either the contaminating water present in the precursor solutions or the generated water through imine bond formation. According to these findings, it is considered that such distortion also occurred in this system. Furthermore, N_2 adsorption isotherm measurements revealed the characteristic gate adsorption behavior at the high pressure ($P/P_0 > 0.9$) and a wide pore size distribution. This may be attributed to mesopores and macropores formed between crystal particles due to the distortion.[45]

Lastly, morphological observation was performed by SEM analysis (Figure S15) clarified that the 2D COFs obtained on the electrode were aggregates of submicrometer-sized particles like TAPB-PDA COF. On the other hand, the TAPM-PDA COF on the electrode appeared to be densely deposited, probably because the TAPM-PDA COF exhibited 3D bottom-up growth onto the electrode, rather than an aggregate structure resulting from bulk growth.

Conclusion

In conclusion, we have demonstrated that the protons generated by the electrolytic oxidation of DPH work as an EGA and promote the imine-bond formation by the condensation reaction of amine and aldehyde monomers giving COF materials. Since the EGA was electrogenerated in the proximity of the electrode surface, the obtained COF materials were successfully immobilized as films onto the electrodes. The obtained COF films were found to have high crystallinity and porosity, and the film thickness could be controlled by modulating the electrolysis time. This synthetic procedure was also applicable for the synthesis of various imine-based COFs, including triazine linkers and 3D structures, on the electrodes. This method using EGA represents a mild and environmentally friendly approach for COF synthesis because it does not require long reaction times, heating conditions, or Lewis acid catalysts, that are necessary in the conventional synthesis of COFs consisting of imine bonds. Moreover, our proposed method, that enables the direct immobilization of COFs onto the electrodes, is expected to be a promising process technique for the application of COFs to devices such as functional modified electrodes and sensing materials.

Acknowledgements

This research was supported by Kakenhi Grant-in-Aid (JP20H02796, JP23H02001 and JP23H04914) from the Japan Society for the Promotion of Science (JSPS), the FOREST Program (Grant Number: JPMJFR211G, Japan) of the Japan Science and Technology Agency (JST) and a Support for Tokyo Tech Advanced Researchers [STAR] Grant funded by the Tokyo Institute of Technology Fund (Tokyo Tech Fund). We acknowledge Dr. Takashi Kajitani (SAXS) Dr. Yoshihisa Sei (CP-MAS ^{13}C NMR) and Dr. Takayuki Kamihara (CP-MAS ^{13}C NMR), Yuka Akimoto (SEM) and Chieko Hara (elemental analysis) at Materials Analysis Division, Open Facility Center, Tokyo Institute of Technology.

Conflict of Interest

The authors declare no conflict of interest.

Data Availability Statement

The data that support the findings of this study are available from the corresponding author upon reasonable request.

Keywords: Covalent Organic Frameworks · Electrode · Electrogenerated Acid · Imine Bond · Porous Film

[1] A. P. Côté, A. I. Benin, N. W. Ockwig, M. O'Keeffe, A. J. Matzger, O. M. Yaghi, *Science* **2005**, *310*, 1166–1170.
[2] T. Ma, E. A. Kapustin, S. X. Yin, L. Liang, Z. Zhou, J. Niu, L.-H. Li, Y. Wang, J. Su, J. Li, X. Wang, W. D. Wang, W. Wang, J. Sun, O. M. Yaghi, *Science* **2018**, *361*, 48–52.
[3] F. Beuerle, B. Gole, *Angew. Chem. Int. Ed.* **2018**, *57*, 4850–4878.
[4] K. Geng, T. He, R. Liu, S. Dalapati, K. T. Tan, Z. Li, S. Tao, Y. Gong, Q. Jiang, D. Jiang, *Chem. Rev.* **2020**, *120*, 8814–8933.
[5] W. Ji, L. Xiao, Y. Ling, C. Ching, M. Matsumoto, R. P. Bisbey, D. E. Helbling, W. R. Dichtel, *J. Am. Chem. Soc.* **2018**, *140*, 12677–12681.
[6] Y. He, X. Lin, J. Chen, Z. Guo, H. Zhan, *ACS Appl. Mater. Interfaces* **2020**, *12*, 41942–41949.

[7] Y. He, X. Lin, Y. Zhou, J. H. Chen, Z. Guo, H. Zhan, *Chem. Mater.* **2021**, *33*, 9413–9424.
[8] J. L. Fenton, D. W. Burke, D. Qian, M. Olvera de la Cruz, W. R. Dichtel, *J. Am. Chem. Soc.* **2021**, *143*, 1466–1473.
[9] H. Ben, G. Yan, H. Liu, C. Ling, Y. Fan, X. Zhang, *Adv. Funct. Mater.* **2022**, *32*, 2104519.
[10] C. Krishnaraj, H. S. Jena, K. S. Rawat, J. Schmidt, K. Leus, V. Van Speybroeck, P. Van Der Voort, *ACS Appl. Mater. Interfaces* **2022**, *14*, 50923–50931.
[11] X. Ao, W. Zhang, Z. Li, J.-G. Li, L. Soule, X. Huang, W.-H. Chiang, H. M. Chen, C. Wang, M. Liu, X. C. Zeng, *ACS Nano* **2019**, *13*, 11853–11862.
[12] D. Chen, S. Huang, L. Zhong, S. Wang, M. Xiao, D. Han, Y. Meng, *Adv. Funct. Mater.* **2020**, *30*, 1907717.
[13] T. B. Schon, B. T. McAllister, P.-F. Li, D. S. Seferos, *Chem. Soc. Rev.* **2016**, *45*, 6345–6404.
[14] B. J. Smith, A. C. Overholts, N. Hwang, W. R. Dichtel, *Chem. Commun.* **2016**, *52*, 3690–3693.
[15] C. Feriante, A. M. Evans, S. Jhulki, I. Castano, M. J. Strauss, S. Barlow, W. R. Dichtel, S. R. Marder, *J. Am. Chem. Soc.* **2020**, *142*, 18637–18644.
[16] C. Kang, K. Yang, Z. Zhang, A. K. Usadi, D. C. Calabro, L. S. Baugh, Y. Wang, J. Jiang, X. Zou, Z. Huang, D. Zhao, *Nat. Commun.* **2022**, *13*, 1370.
[17] M. Matsumoto, R. R. Dasari, W. Ji, C. H. Feriante, T. C. Parker, S. R. Marder, W. R. Dichtel, *J. Am. Chem. Soc.* **2017**, *139*, 4999–5002.
[18] D. Zhu, Y. Zhu, Q. Yan, M. Barnes, F. Liu, P. Yu, C.-P. Tseng, N. Tjahjono, P.-C. Huang, M. M. Rahman, E. Egap, P. M. Ajayan, R. Verduzco, *Chem. Mater.* **2021**, *33*, 4216–4224.
[19] D. N. Bunck, W. R. Dichtel, *J. Am. Chem. Soc.* **2013**, *135*, 14952–14955.
[20] Y. Peng, Y. Huang, Y. Zhu, B. Chen, L. Wang, Z. Lai, Z. Zhang, M. Zhao, C. Tan, N. Yang, F. Shao, Y. Han, H. Zhang, *J. Am. Chem. Soc.* **2017**, *139*, 8698–8704.
[21] S. A. Ahmed, Q. Liao, Q. Shen, M. M. F. Ashraf Baig, J. Zhou, C. Shi, P. Muhammad, S. Hanif, K. Xi, X. Xia, K. Wang, *Chem. Eur. J.* **2020**, *26*, 12996–13001.
[22] G. Li, K. Zhang, T. Tsuru, *ACS Appl. Mater. Interfaces* **2017**, *9*, 8433–8436.
[23] S. Kim, H. Lim, J. Lee, H. C. Choi, *Langmuir* **2018**, *34*, 8731–8738.
[24] D. B. Shinde, G. Sheng, X. Li, M. Ostwal, A.-H. Emwas, K.-W. Huang, Z. Lai, *J. Am. Chem. Soc.* **2018**, *140*, 14342–14349.
[25] P. Shao, J. Li, F. Chen, L. Ma, Q. Li, M. Zhang, J. Zhou, A. Yin, X. Feng, B. Wang, *Angew. Chem. Int. Ed.* **2018**, *57*, 16501–16505.
[26] M. Matsumoto, L. Valentino, G. M. Stiehl, H. B. Balch, A. R. Corcos, F. Wang, D. C. Ralph, B. J. Mariñas, W. R. Dichtel, *Chem* **2018**, *4*, 308–317.
[27] Y. Li, M. Zhang, X. Guo, R. Wen, X. Li, X. Li, S. Li, L. Ma, *Nanoscale Horiz.* **2018**, *3*, 205–212.
[28] M. G. Barnes, D. C. McLeod, R. H. Lambeth, *ACS Appl. Polym. Mater.* **2022**, *4*, 2017–2021.
[29] L. Xu, X. Zhou, Y. Yu, W. Q. Tian, J. Ma, S. Lei, *ACS Nano* **2013**, *7*, 8066–8073.
[30] D. D. Medina, J. M. Rotter, Y. Hu, M. Dogru, V. Werner, F. Auras, J. T. Markiewicz, P. Knochel, T. Bein, *J. Am. Chem. Soc.* **2015**, *137*, 1016–1019.
[31] J. W. Colson, A. R. Woll, A. Mukherjee, M. P. Levendorf, E. L. Spitler, V. B. Shields, M. G. Spencer, J. Park, W. R. Dichtel, *Science* **2011**, *332*, 228–231.
[32] D. D. Medina, V. Werner, F. Auras, R. Tautz, M. Dogru, J. Schuster, S. Linke, M. Döblinger, J. Feldmann, P. Knochel, T. Bein, *ACS Nano* **2014**, *8*, 4042–4052.
[33] T. Sick, A. G. Hufnagel, J. Kampmann, I. Kondofersky, M. Calik, J. M. Rotter, A. Evans, M. Döblinger, S. Herbert, K. Peters, D. Böhm, P. Knochel, D. D. Medina, D. Fattakhova-Rohlfing, T. Bein, *J. Am. Chem. Soc.* **2018**, *140*, 2085–2092.
[34] L. Wang, C. Zeng, H. Xu, P. Yin, D. Chen, J. Deng, M. Li, N. Zheng, C. Gu, Y. Ma, *Chem. Sci.* **2019**, *10*, 1023–1028.
[35] X. Wang, J. Yang, X. Shi, Z. Zhang, C. Yin, Y. Wang, *Small* **2022**, *18*, 2107108.
[36] J. M. Rotter, S. Weinberger, J. Kampmann, T. Sick, M. Shalom, T. Bein, D. D. Medina, *Chem. Mater.* **2019**, *31*, 10008–10016.
[37] E. Tavakoli, A. Kakekhani, S. Kaviani, P. Tan, M. M. Ghaleni, M. A. Zaeem, A. M. Rappe, S. Nejati, *J. Am. Chem. Soc.* **2019**, *141*, 19560–19564.
[38] L. Wang, C. Xu, W. Zhang, Q. Zhang, M. Zhao, C. Zeng, Q. Jiang, C. Gu, Y. Ma, *J. Am. Chem. Soc.* **2022**, *144*, 8961–8968.
[39] N. Kise in *Encyclopedia of Applied Electrochemistry* (Eds.: G. Kreysa, K. Ota, R. F. Savinell), Springer, New York, **2014**, pp. 702–706.
[40] K. Maurer, A. McShea, M. Strathmann, K. Dill, *J. Comb. Chem.* **2005**, *7*, 637–640.
[41] M. Kongsfelt, J. Vinther, K. Malmos, M. Ceccato, K. Torbensen, C. S. Knudsen, K. V. Gothelf, S. U. Pedersen, K. Daasbjerg, *J. Am. Chem. Soc.* **2011**, *133*, 3788–3791.
[42] J. Vinther, J. Iruthayaraj, K. Gothelf, S. U. Pedersen, K. Daasbjerg, *Langmuir* **2013**, *29*, 5181–5189.
[43] T. Ma, J. Li, J. Niu, L. Zhang, A. S. Etman, C. Lin, D. Shi, P. Chen, L.-H. Li, X. Du, J. Sun, W. Wang, *J. Am. Chem. Soc.* **2018**, *140*, 6763–6766.
[44] D. M. Fischbach, G. Rhoades, C. Espy, F. Goldberg, B. J. Smith, *Chem. Commun.* **2019**, *55*, 3594–3597.
[45] W. Gao, X. Sun, H. Niu, X. Song, K. Li, H. Gao, W. Zhang, J. Yu, M. Jia, *Microporous Mesoporous Mater.* **2015**, *213*, 59–67.

Manuscript received: May 25, 2023
Accepted manuscript online: June 9, 2023
Version of record online: July 3, 2023